MAS-Based Energy Management Strategies for a Hybrid Energy Generation System

Junzhi Yu, *Senior Member, IEEE*, Chunxia Dou, and Xinbin Li

***Abstract*—An advanced control scheme for managing a hybrid energy generation system (HEGS) is presented in this paper. A hierarchical management and control architecture based on multi-agent systems (MAS) is discussed. MAS will account for the complex behavior of a hybrid energy supply system. The management and control strategies are implemented through a system of agents based on three tiers. The upper level agents develop overall energy management strategies for a hybrid energy supply system. The middle-level agents integrate coordinated switching controllers. The lower level agents are responsible for dealing with local control strategies. Coordinated switching controllers within the middle-level agents are designed as event-triggered hybrid controllers based on differential hybrid Petri-net (DHPN) models. The operation modes of distributed energy resources (DERs) can smoothly transfer in a coordinated manner due to the coordinated action of the switching controllers according to variation in operating conditions. Finally, simulation results from different scenarios verifying the feasibility of the proposed scheme are offered.**

***Index Terms*—Control strategies, energy management, event-triggered hybrid control, hybrid energy generation system (HEGS), multi-agent system (MAS).**

Nomenclature

CCA	Coordinated control agent.
DERs	Distributed energy resources.
DHPN	Differential hybrid Petri-net.
EMA	Energy management agent.
EMS	Energy management system.
FIPA	Foundation for intelligent physical agents.
HEGS	Hybrid energy generation system.
MAS	Multi-agent system.
MPPT	Maximum power point tracking.
PV	Photovoltaic.
SOC	State of charge.
UA	Unit agent.
UC	Ultracapacitor.
WT	Wind turbine.

Manuscript received September 11, 2015; revised December 12, 2015; accepted January 12, 2016. Date of publication February 3, 2016; date of current version May 10, 2016. This work was supported in part by the National Natural Science Foundation of China under Grant 61573300, Grant 61172095, and Grant 61375102, and in part by the Beijing Natural Science Foundation under Grant 4161002. *(Corresponding author: Junzhi Yu.)*

J. Yu is with the State Key Laboratory of Management and Control for Complex Systems, Institute of Automation, Chinese Academy of Sciences, Beijing 100190, China (e-mail: junzhi.yu@ia.ac.cn).

C. Dou and X. Li are with the Institute of Electrical Engineering, Yanshan University, Qinhuangdao 066004, China (e-mail: cxdou@ysu.edu.cn; lixb@ysu.edu.cn).

Color versions of one or more of the figures in this paper are available online at http://ieeexplore.ieee.org.

Digital Object Identifier 10.1109/TIE.2016.2524411

I. Introduction

RECENTLY, the use of renewable energy has been regarded as an effective way of solving energy outages and environment pollution problems [1], [2]. However, a single type of renewable energy resource typically cannot meet load supply requirements. Renewable sources rely on generation from the sun and wind. Due to the intermittent and stochastic nature of wind speed and solar irradiation, renewable sources are not always available to meet demand. In order to make use of available renewable energy sources, HEGS integrate various types of small DERs. Resources such as WTs, PV arrays, and batteries are classified as DERs. HEGS are widely regarded for utilizing renewable energy resources. HEGS can meet load demand with high reliability and at moderate costs provided the system is managed effectively [3], [4]. However, management and control of HEGS are a challenging problem for the following reasons.

1) HEGS consists of different types of DERs resulting in a complex structure.
2) DERs present a mixture of operational patterns, including time-continuous dynamics and event-driven discrete behaviors. Both patterns may interact with each other [5], [6].
3) The availability of renewable energy generation is usually intermittent and unpredictable [7].
4) DERs operate in multiple modes and may need to switch modes in response to environmental changes [8].

In a complex HEGS, a proper EMS is essential for optimizing cost effectiveness [9]. Additionally, an intelligent control strategy is also necessary to ensure a reliable and flexible energy supply system [10], [11]. Consequently, taking into account the multiple objectives regarding energy management and intelligent control, a hierarchical management and control architecture based on MAS are proposed in this paper.

Many studies related to energy management of HEGS are based on distributed multi-agents methods [12]–[15]. In [13], an energy optimization management problem was solved by using MAS by taking into account four types of operation modes and switching relationships. Further, References [14] and [15] were mainly focused on methods for switching between operation modes of storage units by using MAS-based fuzzy-logic rules for ensuring better system reliability. From the above-mentioned studies, we can conclude that system

reliability can be significantly improved when using an intelligent controller which switches between modes in response to operational changes. However, in these studies, the switching controller is used only for energy storage units. Therefore, the logic judgments are not very complicated. Renewable energy units such as PV and WT have multiple operation modes [16]. The logical relationships behind these modes are occasionally complex. Moreover, these DER units need to comply with logical relationships to switch their operation modes in a coordinated manner. To meet these requirements, the following original strategy is proposed in this paper.

1) Middle-level CCAs are added in order to implement the switching control between operation modes between DERs to ensure the energy supply system is reliable and flexible.
2) A switching control system based on a DHPN model is proposed to fully model hybrid behaviors and logical relationships of the operation modes of all DERs. Note that switching controls will be triggered based on violation of constraint conditions, thus called as event-triggered switching controls. The switching controls are designed according to different event-triggered conditions and can be divided in three main types: the first is a switching control within an agent; the second type is a coordinated switching control; the final type is an inhibitive switching between agents. Thus, the switching controls are also called an event-triggered hybrid switching control.
3) In the DHPN model, the enabling functions associated with arcs define the operational constraint conditions and the logical relationships among the operational modes. The three types of switching controls are designed, respectively, by means of different enabling functions. The switching controls must comply with the system constraints while also swapping operation modes in a coordinated manner.
4) The proposed energy management strategy is a centralized method implemented by means of MASs. Each agent can locally process the constraints of their respective units by means of the internal switching control as discussed in Section IV. The unit constraints can then be locally controlled within an allowable range. Therefore, only the constraint condition of the entire system requires consideration when resolving optimization concerns. The proposed method reduces both computational and communication burden simultaneously when compared to conventional centralized management techniques where the central controller must process a number of constraints.

Our research is prepared using the following approach.

1) A MAS-based three-level management and control scheme is built by using a three-tier agent format.
2) The design of the energy optimization management strategy takes into account the interactions between the upper level agent and other agents.
3) Event-triggered hybrid switching controls are considered when designing the middle-level control agent.
4) The lower level agent responsible for system stability accounts for different dynamic behaviors of DERs.

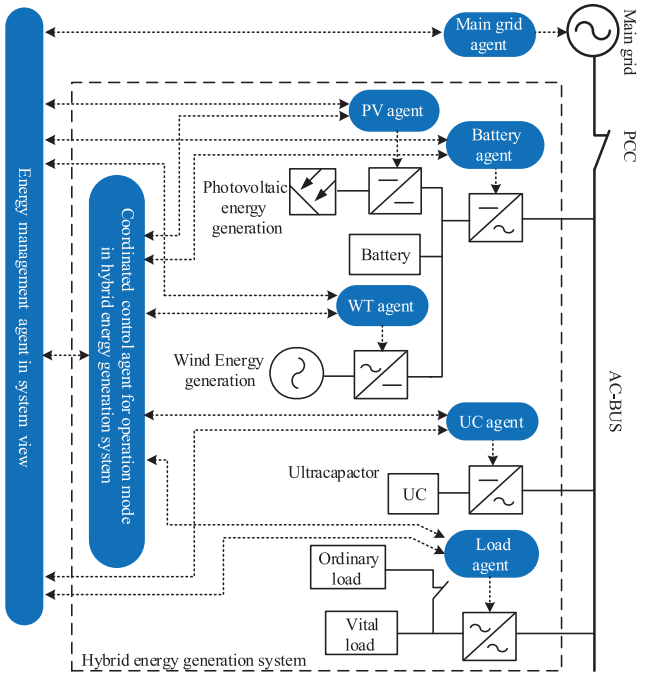

Fig. 1. MAS-based hierarchical management and control scheme.

5) The validity of the proposed scheme is shown by presenting numerical simulation results.

We initially propose the MAS-based hierarchical control as described in Section II. We then proceed to develop energy management, switching control, as well as local control strategies as presented in Sections III, IV and V, respectively. The simulation tests are presented in Section VI. Finally, Section VII gives some concluding remarks.

II. MAS-Based Hierarchical Control

Fig. 1 shows a HEGS connected to the main grid containing PV, WT, battery, and an UC including critical and noncritical loads. The decision making process of each DER unit or load is carried out by their respective agent. The middle-level agent executes the coordinated switching control functions, while the upper level agent energy resolves the overall system optimization concerns. Fig. 2 shows the structure of the proposed hierarchical MAS.

The upper level agent, as shown in Fig. 2, is designed as a deliberative agent whose goal is to optimize the cost effectiveness of the entire system. The optimization model is developed in the process module by using real-time data. The energy management strategies are determined in the decision-making module and executed through the action implementation module. The time scale of the optimization process assumes an hourly basis.

The middle-level agent is also designed as a deliberative agent with the objective to switch operational modes between agents to ensure a reliable and flexible energy supply. The point of common coupling (PCC) voltage level is assessed in the security assessment module based on real-time data. The coordinated switching controls are designed in the decision making module and executed by the action implementation module.

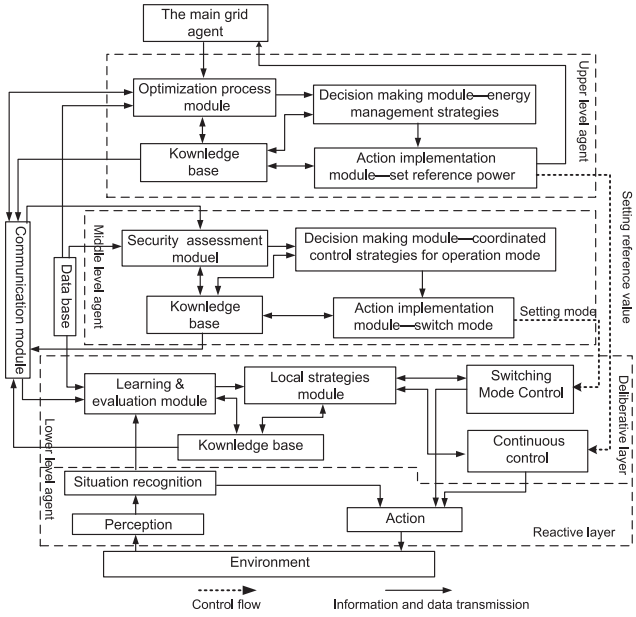

Fig. 2. Structure of the hierarchical MAS.

The time scale of the switching control is based on hour or minute level.

All lower level agents are designed as hybrid agents, which are composed of reactive and deliberative layers. The reactive layer is defined as the recognition, perception, and action layer and has priority to respond quickly to environmental emergencies. The deliberative layer is defined as the belief, desire, and intention layer has high intelligence to plan the action of the agent to achieve the required goals. According to the reference power value set by the upper level agent and the operation mode set by the middle-level agent; the local control strategies in the deliberative layer are designed. The time scale of the local control is based on the second level.

In the hierarchical MAS, the interaction among agents is divided into two categories, direct and indirect interactions. When one agent responds to a cooperation request of another agent, this is an example of direct interaction. When an agent modifies the environment of another agent, this is an example of indirect interaction. When using the MAS-based hierarchical scheme, handling complex energy management problems for HEGS mainly depends on energy management strategies, coordinated switching controls, and local control strategies. The management and control strategies that will be detailed later are implemented through three-level agents in an interactive manner.

III. Energy Management Strategies

This section focuses on design and implementation of energy management strategies through the interaction between the upper level agent and other agents.

A. Design of Energy Management Strategies

The energy optimization problem can be formulated as the following objective function, which satisfies the constraint:

$$O_s = \min\Big\{\beta_1\Big\{C_g P_g + \sum_{i=1}^{4}\varphi_{is}[h_i F_{is}(P_{\text{DER}is}) + M_i(P_{\text{DER}is}) + \lambda_{is}C_{sti}]\Big\} + \beta_2[f_g P_g + \sum_{i=1}^{4}\sum_{s=1}^{S}\varphi_{is} f_{is} P_{\text{DER}is}]\Big\}$$
$$\text{s.t.} \quad P_g + \sum_{i=1}^{4}\varphi_{is} P_{\text{DER}is} = P_{\text{load}} \tag{1}$$

where $i \in \{1,2,3,4\}$ is the number of DERs in the HEGS; s indicates the operation mode; P_g is the active power from the main grid to the HEGC; C_g is the cost per unit and f_g is the power quality coefficient of the main grid; $P_{\text{DER}_{is}}$ is the active power of the ith DER unit in the sth mode; $F_{is}(P_{\text{DER}_{is}})$ denotes the consumption characteristic function; h_i is the fuel price per unit; $M_i(P_{\text{DER}_{is}})$ is the maintenance cost, which is deemed in proportion to $P_{\text{DER}_{is}}$; C_{sti} is the starting cost; $\lambda_{is} \in \{0,1\}$, $\lambda_{is} = 1$ when the ith DER unit is in starting state; otherwise, $\lambda_{is} = 0$; $\phi_{is} \in \{0,1\}$ 1 for the operating mode and 0 for the stopping mode; f_{is} is the power quality coefficient of the ith DER unit in the sth mode; β_1 and β_2 are the respective weights of the economic and quality indices; and P_{load} is the sum of loads in the HEGS.

In the function above there is only one constraint condition since the constraint conditions of each DER unit are satisfied by their local agent. Hence, the requirements regarding computation and communications matters decrease when resolving optimization issues. This matter is discussed further in Section IV.

Coefficients of (1) can be acquired by using system technical information and real-time data. The optimization problem is then solved by using an improved particle swarm optimization method presented in [17]. With respect to the particle swarm optimization, in the iteration formula regarding position and velocity of particle, there is an inertial weight factor used to control the convergence behavior of the particle swarm optimization. Larger values of the inertial weight factor enable the algorithm to avoid being entrapped in a local minimum but easy to result in a very slow convergence. Therefore, the inertial weight factor plays a role of balancing convergence and exploration ability. To satisfy the real-time requirement, also to avoid falling into a local minimum, when dealing with the upper level optimization problem, the inertial weight factor can be dynamically adjusted and linearly decreased during the iterations by using the improved particle swarm optimization method. In other words, by means of the improved particle swarm optimization method, the optimum resolution can be achieved rapidly without falling into a local minimum. The resolution of the optimization problem determines the power dispatched by the DERs.

B. Interaction Between Upper Level Agents and Other Agents

Energy management strategies are implemented through the interactions between the EMA and other agents. These strategies are based on the FIPA—agent communication language (FIPA-ACL) in JADE [18]. FIPA-ACL messages are characterized by performativity, conversation ID, content, and receivers. When the operation mode of the HEGS is switched, the EMA starts and reassigns the power to be dispatched by all DERs.

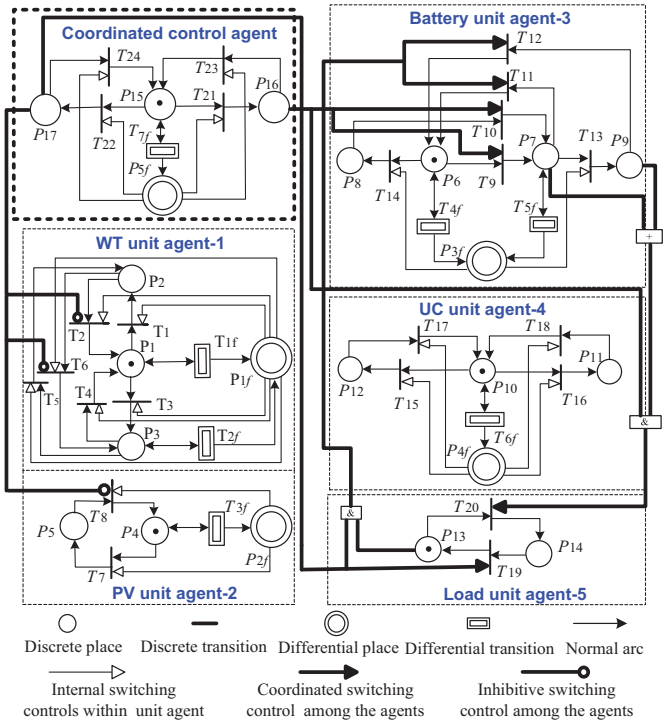

Fig. 3. Event-triggered hybrid switching controls based on DHPN.

IV. Event-Triggered Hybrid Switching Control

The middle-level agent includes coordinated switching controls of operation modes to respect the hybrid behaviors of DERs and the logical relationship of their modes. The event-triggered hybrid switching controls are then designed for the hybrid models of all DERs. The DHPN model is known as one of the best modeling methods of complex hybrid systems [19]–[21]. Thus, a DHPN model is developed to describe the hybrid behaviors of the HEGS.

A. DHPN-Based Hybrid Model

From Fig. 1, the HEGS is modeled as a DHPN model as shown in Fig. 3, consisting of four DER units submodels, one load submodel, and one coordinated control submodel. The DHPN model is defined by a 14 tuple $(P_D, T_D, P_{DF}, T_{DF}, X, A_N, A_I, A_T, P_{\text{re}}, P_{\text{os}}, \Gamma, H, I, M_0)$,
where

$P_D \in \{P_1, P_2, \ldots, P_{17}\}$ is a set of discrete places, which represents the operation modes of all units;
$T_D \in \{T_1, T_2, \ldots, T_{24}\}$ is a set of discrete transitions, which represents the event-triggered switching behaviors;
$P_{DF} \in \{P_{1f}, P_{2f}, \ldots, P_{5f}\}$ is a set of continuous places, which describes the continuous states of all units;
$T_{DF} \in \{T_{1f}, T_{2f}, \ldots, T_{7f}\}$ is a set of continuous transitions, which represents the dynamic behaviors;
$P = P_D \cup P_{DF}$, $T = T_D \cup T_{DF}$, $P \cap T = \phi$, $P \cup T \neq \phi$;
$X = [x_1, x_2, \ldots, x_n]^T$ is the state vector of P_{DF};
$A_N \subseteq ((P_D \times T_D) \cup (T_D \times P_D)) \cup ((P_D \times T_{DF}) \cup (T_{DF} \times P_D))$ is a set of normal arcs of the DHPN;
$A_I \subseteq (P_D \times T_D)$ is a set of inhibitor arcs;

TABLE I
Description of Discrete Places

Discrete places	Description
P_1	MPPT operation mode of the WT unit
P_2	Stopping mode of the WT unit
P_3	Constant power output operation mode of the WT unit
P_4	MPPT operation mode of the PV unit
P_5	Stopping mode of the PV unit
P_6	Charging operation mode of the battery unit
P_7	Discharging operation mode of the battery unit
P_8	Stopping mode of the battery with SOC
P_9	Stopping mode of the battery with minimal SOC
P_{10}	Normal voltage mode of the UC unit
P_{11}	Lower voltage mode of the UC unit
P_{12}	Higher voltage mode of the UC unit
P_{13}	Full load operation mode of the load unit
P_{14}	Shedding load mode of the load unit
P_{15}	Normal operation mode of the PCC voltage
P_{16}	low voltage operation mode of the PCC voltage
P_{17}	high voltage operation mode of the PCC voltage

$A_T \subseteq (P_D \times T_D) \cup (P_{DF} \times T_D)$ is a set of test arcs;
P_{re} and P_{os} are defined as predecessor and posterior function associated with the normal arc, respectively;
Γ is a timing map for the discrete transients, by which the minimal switching interval can be defined.
$H_{DF}(P_{if}, T_j)$ is defined as enabling function associated with the test arc that connects the ith differential preplace to the jth discrete transition;
$H_D(P_i, T_j)$ is defined as enabling function associated with the test arc that connects the ith discrete preplace to the jth discrete transition;
$I_D(P_i, T_j)$ is defined as enabling function associated with the inhibitor arc that connects the ith discrete preplace to the jth discrete transition;
$M_0 \in \{M_{10}, M_{20}, \ldots, M_{60}\}$ is the initial mode of the six UAs.

The detailed descriptions regarding the places and transitions corresponding to Fig. 3 are shown in Tables I–IV.

All normal arcs are described with a small arrow as "$\rightarrow$" in Fig. 3. The functions associated with all normal arcs $P_{\text{re}}(P_i, T_j)$, $P_{\text{os}}(P_i, T_j)$, $P_{\text{re}}(P_i, T_{kf})$, and $P_{\text{os}}(P_i, T_{kf})$ are defined as "logical 0," where $i = 1, 2, \ldots, 17$, $j = 1, 2, \ldots, 24$, and $k = 1, 2, \ldots, 7$.

The initial operation mode of each unit is denoted by a token. The first mode is defined as "1" in the initial marking with a black dot in Fig. 3. The other modes without tokens are defined as "0" in the initial marking. When the operation mode is switched, the token is transformed from the preplace into a corresponding postplace. In the DHPN model, the initial markings of all units are as follows: $M_{10}(P_1, P_2, P_3) = [1, 0, 0]$, $M_{20}(P_4, P_5) = [1, 0]$, $M_{30}(P_6, P_7, P_8, P_9) = [1, 0, 0, 0]$, $M_{40}(P_{10}, P_{11}, P_{12}) = [1, 0, 0]$, $M_{50}(P_{13}, P_{14}) = [1, 0]$, $M_{60}(P_{15}, P_{16}, P_{17}) = [1, 0, 0]$.

In order to understand the DHPN model better and take the battery submodel as an example, some explanations are offered as follows. 1) The battery unit has four operation modes: charging mode described as P_6, discharging mode described as

TABLE II
DESCRIPTION OF DISCRETE TRANSITIONS

Discrete transition	Description
T_1	Switch the WT unit to stopping mode from MPPT mode
T_2	Switch the WT unit to MPPT mode from stopping mode
T_3	Switch the WT unit to constant output mode from MPPT mode
T_4	Switch the WT unit to MPPT mode from constant output mode
T_5	Switch the WT unit to stopping mode from constant output mode
T_6	Switch the WT unit to constant output mode from stopping mode
T_7	Switch the PV unit to stopping mode from MPPT mode
T_8	Switch the PV unit to MPPT mode from stopping mode
T_9	Switch the battery unit to discharging mode from charging mode
T_{10}	Switch the battery unit to discharging mode from stopping mode with the maximal SOC
T_{11}	Switch the battery unit to charging mode from discharging mode
T_{12}	Switch the battery unit to charging mode from stopping mode with the minimal SOC
T_{13}	Stop the battery discharging because SOC reaches to the minimal value
T_{14}	Stop the battery charging because SOC reaches to the maximal value
T_{15}	Switch the UC to higher voltage operation mode
T_{16}	Switch the UC to lower voltage operation mode
T_{17}	Switch the UC to normal voltage operation mode form higher voltage mode
T_{18}	Switch the UC to normal voltage operation mode form lower voltage mode
T_{19}	Inform load restored
T_{20}	Inform load shedding
T_{21}	Inform that the PCC voltage is in low-voltage mode
T_{22}	Inform that the PCC voltage is in high-voltage mode
T_{23}	Inform that the PCC voltage has returned into normal mode from low-voltage mode
T_{24}	Inform that the PCC voltage has returned into normal mode from high voltage mode

TABLE III
DESCRIPTION OF DIFFERENTIAL PLACES

Differential places	Description
P_{1f}–P_{4f}	Continuous states of the generation units1–4
P_{5f}	Continuous states of the PCC voltage

TABLE IV
DESCRIPTION OF DIFFERENTIAL TRANSITIONS

Differential transitions	Description
T_{1f} and T_{2f}	Dynamic behaviors of the WT unit in P_1 and P_3 respectively
T_{3f}	Dynamic behavior of the PV unit in P_4
T_{4f} and T_{5f}	Dynamic behaviors of the battery unit in P_6 and P_7 respectively
T_{6f}	Dynamic behavior of the UC unit in P_{10}
T_{7f}	Dynamic behavior of the PCC voltage

P_7, stopping mode with maximal SOC described as P_8, and stopping mode with minimal SOC described as P_9. 2) The logic switching behaviors among four modes are described by $T_9 - T_{14}$. 3) The continuous states of the battery unit are described by P_{3f}. 4) Corresponding to both charging and discharging operating modes, the dynamic behaviors are described by $T_4 f$ and $T_5 f$, respectively. 5) The initial mode of the battery unit is charging mode. The descriptions of other units are in a similar fashion. The hybrid behavior of the HEGS can be determined using the definitions provided above. Further, the event-triggered hybrid switching controllers can be designed as well.

Each discrete transition in the DHPN model needs to be triggered by the enabling function of the test or inhibitor arc connected into the transition. The test arcs are designed following two forms: $(P_{DF} \times T_D)$ and $(P_D \times T_D)$, which are described as "—▷ " and "➞" respectively, in Fig. 3. The inhibitor arcs are only designed by one kind: $(P_D \times T_D)$ described as "⊸ ." The enabling functions of different arcs define the constraint conditions or can describe logical relationships behind the operational mode. Once a constraint condition is violated, the enabling function is activated (logical "1" from "0") to trigger the transition connected with its arc, so that corresponding operation mode is switched.

Therefore, the switching controls of the operational mode can be designed by means of these enabling functions. That is, through designing constraint conditions or reasonable logical relationships of the enabling functions, the operation modes can be switched in a coordinated way. Corresponding to the enabling functions associated with three kinds of arcs, the switching controls are also designed according to three categories.

1) *Internal switching controls* in each UA, which are designed by means of the enabling functions of the test arcs "—▷".
2) *Coordinated switching controls* among UAs, which are designed by means of the enabling functions of the test arcs "➞".
3) *Switching inhibitive controls* among the agents, which are designed by means of the enabling functions of the inhibitive arcs "⊸ ." When the enabling function becomes "logical 1," the discrete transition connected with its arc is triggered. This allows switching the corresponding operational mode. Hence, the switching controls are called event-triggered hybrid controls. The detailed design is provided below.

B. Internal Switching Control in Each Agent

In the DHPN model, $H_{DF}(P_{if}, T_j)$ is defined as the enabling function of the test arc that connects a differential preplace to a discrete transition. The test arc is indicated as "—▷" in Fig. 3. The internal switching control is designed by means of this enabling function according to the constraint condition of each agent. Once the constraint condition of P_{if} is violated, the enabling function $H_{DF}(P_{if}, T_j)$ is then activated (becomes "logical 1" from "0") to trigger the transition T_j. At the moment the switching event of T_j occurs, the corresponding operation mode is switched. Therefore, the switching controls are driven by the violation of the constraint condition resulting in the internal mode switching of each agent. Specifically, $H_{DF}(P_{if}, T_j)$ is defined as follows.

For the WT UA

$$\text{when } v \text{ drops to } v \le v_{\text{ci}} \text{ from } v_{\text{ci}} < v \le v_R, H_{DF}(P_{1f}, T_1) = 1 \tag{2}$$

when v rises to $v_{ci} < v \leq v_R$ from $v \leq v_{ci}, H_{DF}(P_{1f}, T_2) = 1$ (3)

when v rises to $v_R < v \leq v_{co}$ from $v_{ci} < v \leq v_R, H_{DF}(P_{1f}, T_3) = 1$ (4)

when v rises to $v > v_{co}$ from $v_R < v \leq v_{co}, H_{DF}(P_{1f}, T_5) = 1$ (5)

when v drops to $v_R < v \leq v_{co}$ from $v > v_{co}, H_{DF}(P_{1f}, T_6) = 1$ (6)

when v drops to $v_{ci} < v \leq v_R$ from $v_R < v \leq v_{co}, H_{DF}(P_{1f}, T_4) = 1$ (7)

otherwise, $H_{DF}(P_{1f}, T_i) = 0 (i = 1, 2, \ldots, 6)$

where v is the wind speed; v_{ci} is the cut-in wind speed; v_{co} is the cut-off wind speed; and v_R is the rated wind speed.

With regard to the PV UA

when G_{ing} drops to $G_{\text{ing}} \leq \text{C}$ from $G_{\text{ing}} > \text{C}, H_{DF}(P_{2f}, T_7) = 1$ (8)

when G_{ing} rises to $G_{\text{ing}} > \text{C}$ from $G_{\text{ing}} \leq \text{C}, H_{DF}(P_{2f}, T_8) = 1$ (9)

otherwise, $H_{DF}(P_{2f}, T_i) = 0 (i = 7, 8)$

where G_{ing} is the incident irradiance and C is the threshold value.

Regarding the battery agent

when SOC drops to $\text{SOC} \leq \text{SOC}_{\min}, H_{DF}(P_{3f}, T_{13}) = 1$ (10)

when SOC rises to $\text{SOC} \geq \text{SOC}_{\max}, H_{DF}(P_{3f}, T_{14}) = 1$ (11)

otherwise, $H_{DF}(P_{3f}, T_i) = 0 (i = 13, 14)$

where SOC is the state of charge; $\text{SOC}_{\max}$ and $\text{SOC}_{\min}$ are the maximum and minimum SOC, respectively.

In the UC UA

when U drops to $U \leq U_{\min}, H_{DF}(P_{4f}, T_{16}) = 1$ (12)

when U rises to $U_{\max} > U > U_{\min}, H_{DF}(P_{4f}, T_{18}) = 1$ (13)

when U rises to $U \geq U_{\max}, H_{DF}(P_{4f}, T_{15}) = 1$ (14)

when U drops to $U_{\min} < U < U_{\max}, H_{DF}(P_{4f}, T_{17}) = 1$ (15)

otherwise, $H_{DF}(P_{4f}, T_i) = 0 \ (i = 15, 16, 17, 18)$

where U is the voltage of the UC; $U_{\min}$ is the minimal voltage threshold value; and $U_{\max}$ is the maximal voltage threshold value.

In the CCA

when U_{PCC} drops to $U_{\text{PCC}} \leq U_{\text{Pmin}}, H_{DF}(P_{5f}, T_{21}) = 1$ (16)

when U_{PCC} rises to $U_{\text{Pmax}} > U_{\text{PCC}} > U_{\text{Pmin}}, H_{DF}(P_{5f}, T_{23}) = 1$ (17)

when U_{PCC} rises to $U_{\text{PCC}} \geq U_{\text{Pmax}}, H_{DF}(P_{5f}, T_{22}) = 1$ (18)

when U_{PCC} drops to $U_{\text{Pmin}} < U_{\text{PCC}} < U_{\text{Pmax}}, H_{DF}(P_{5f}, T_{24}) = 1$ (19)

otherwise, $H_{DF}(P_{5f}, T_i) = 0 (i = 21, 22, 23, 24)$

where U_{PCC} is the PCC voltage; and U_{Pmin} and U_{Pmax} are the minimal and maximal threshold values of the PCC voltage, respectively.

In Fig. 3, all of the above switching controls represented by enabling functions are properly developed.

C. Coordinated Switching Control Among Agents

$H_D(P_i, T_j)$ is defined as the enabling function of a test arc that connects a discrete preplace to a discrete transition, and the test arc is indicated as "→" in Fig. 3. The coordinated switching controls among agents are designed by means of the enabling function $H_D(P_i, T_j)$ according to the security assessment of the PCC voltage. The coordinated switching controls are driven by the security assessment of the PCC voltage and result in mode switching between the agents.

Based on the defined logical relationships of the operational modes, i.e.,

$$\bar{P} = P_6(P_7 + P_9) \text{ and } \tilde{P} = P_{13}P_{17}. \quad (20)$$

$H_D(P_i, T_j)$ can be designed as follows.

When the PCC voltage is in low-voltage mode

$$H_D(P_{16}, T_9) = 1 \text{ and } H_D(P_{16}, T_{10}) = 1. \quad (21)$$

When the PCC voltage is in low-voltage mode and the battery unit is in discharge mode or in stopping mode with minimal SOC

$$H_D(\bar{P}, T_{20}) = 1. \quad (22)$$

When the PCC voltage is in high-voltage mode

$$H_D(P_{17}, T_{19}) = 1. \quad (23)$$

When the PCC voltage is in high-voltage mode and the load unit is in full-load mode

$$H_D(\tilde{P}, T_{11}) = 1 \text{ and } H_D(\tilde{P}, T_{12}) = 1. \quad (24)$$

Otherwise, this kind of enabling function is zero.

Note that in Fig. 3, all the coordinated switching controls designed by this type of enabling functions should be empirically designed.

D. Inhibitive Switching Among Agents

$I_D(P_i, T_j)$ is defined as the enabling function associated with an inhibitor arc. The arc is designated as "⊸" in Fig. 3.

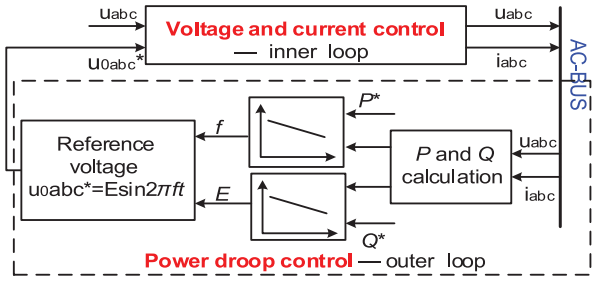

Fig. 4. P/Q droop control scheme of an agent.

The inhibitive switching between the agents is designed by this type of enabling function. $I_D(P_i, T_j)$ is defined as follows.

When the PCC voltage is in high-voltage mode, it follows that:

$$I_D(P_{17}, T_2) = 1, I_D(P_{17}, T_6) = 1, \text{and } I_D(P_{17}, T_8) = 1. \tag{25}$$

Otherwise, this kind of enabling function is zero.

The inhibitive switching resulting from the enabling functions is described when the PCC is determined to be in high-voltage mode and T_2, T_6, and T_8 are restricted. Even if T_2, T_6, and T_8 are triggered by the internal switching control, the corresponding operation modes still cannot be switched. The purpose of this restriction is to prevent the PCC voltage from deteriorating further.

V. Local Control Strategies

The lower level agent is mainly responsible for stability performance of its distributed generation unit through local control strategies.

The control structure of the UA is shown in Fig. 4. The active/reactive power reference values of the controller are set by the upper level EMA, and the operation mode of the controller is set by the middle-level CCA. Each distributed generation inverter has an outer power loop based on droop control whose purpose is to share active and reactive power between distributed generation units. Additionally, the outer power loop with droop control improves the system stabilization performance and adjusts both the frequency and magnitude of the output voltage. The real active/reactive powers are calculated by using the output voltage and current. Then errors between the active/reactive power references and the real active/reactive powers act as the inputs of the droop controllers, respectively.

In low-voltage HEGS, the line impedance is highly resistive, so that the droop control can be determined as [22], [23]

$$f - f_0 = k_q(Q - Q^*) \tag{26}$$

$$E - E_0 = k_p(P - P^*) \tag{27}$$

where f and E are the frequency and the amplitude of the output voltage, respectively; K_p and k_q define the corresponding slope coefficients; and P^* are Q^* denote active/reactive power references.

The voltage reference is obtained through the droop control, which acts as the reference input of inner loop voltage/current control. Considering the uncertainty and multimode characteristics, the $H\infty$ robust control method based on multiply Lyapunov's function is proposed to design the inner loop controller. The method has been introduced in detail in [24] and [25].

VI. Simulation Results

For a typical summer day, corresponding to the time from 8 to 24 h, the ordinary load and the vital load demands are shown in Fig. 5(a) for the simulated HEGS as shown in Fig. 1. The wind speed and sun irradiance are shown in Fig. 5(b) and are real measurement data. In the HEGS, the battery is used for larger long-term energy compensation, and UC is sized only for providing smaller transient power regulation. Therefore, the battery and UC units are considered as storage units. Using three switching control schemes, i.e., the logical judgment similar to [14]; the fuzzy-logical rule similar to [15]; and the proposed scheme in this paper; the active power dispatch from three distributed generation units and the main grid are shown in Fig. 5(c)–(e), respectively. The active power outputs are shown in Fig. 5(f) which corresponds to the power dispatch under the proposed scheme described in this paper. Additionally, the PCC voltage and frequency performance under the three kinds of schemes are shown in Fig. 5(g) and (h). Notice that the time scale is from 8 to 24 h. During 0 to 8 h, the load is minimal so that switching controllers barely function.

From Fig. 5(c)–(e), it can be seen that PV and WT units do not run in MPPT mode during most of the simulation time under the first two schemes. This is due to the two schemes focusing on the logical switching of the storage unit without taking into account the coordinated logical relationship among the battery, PV, and WT units. As a result, PV and WT energy generation cannot be fully used. Therefore, the main grid provides a larger power supply with a corresponding higher operating cost. However, under the proposed management and control scheme, PV and WT units run in MPPT mode during most of the simulation time. Only when the incident irradiance is lower than the threshold value, or wind speed drops lower than the cut-in speed, do the two units switch to stopping mode. Hence, when the PV and WT units are running at full capacity, the main grid is providing less power. Approximately, from 12:15 P.M. to 16:15 P.M., PV and WT provide surplus power to the main grid based on demand. As a result, the operating cost of the system is lower. From Fig. 5(f), it is observed that using the proposed schemes, the real power outputs of all DERs are being regulated effectively, so that the system unbalanced power is very small. From Fig. 5(g) and (h), it can be seen that a load suddenly connected at the 17:30 P.M. leads to a sharp drop of the PCC voltage and frequency. By using the first two schemes before 17:30 P.M., the PCC voltage and frequency are controlled within the proper range. However, after the 17:30 P.M., the PCC voltage decreases to a value lower than 0.94 p.u., and the frequency drops down to a value lower than 0.96 p.u. This is due to the switching operational mode of the storage unit. Hence, the voltage and frequency cannot be recovered quickly. From Fig. 5(g) and (h), it can be also seen that by using the proposed schemes, even if at the instant of 17:30 P.M., the suddenly connected load also leads to a sharp decline of the

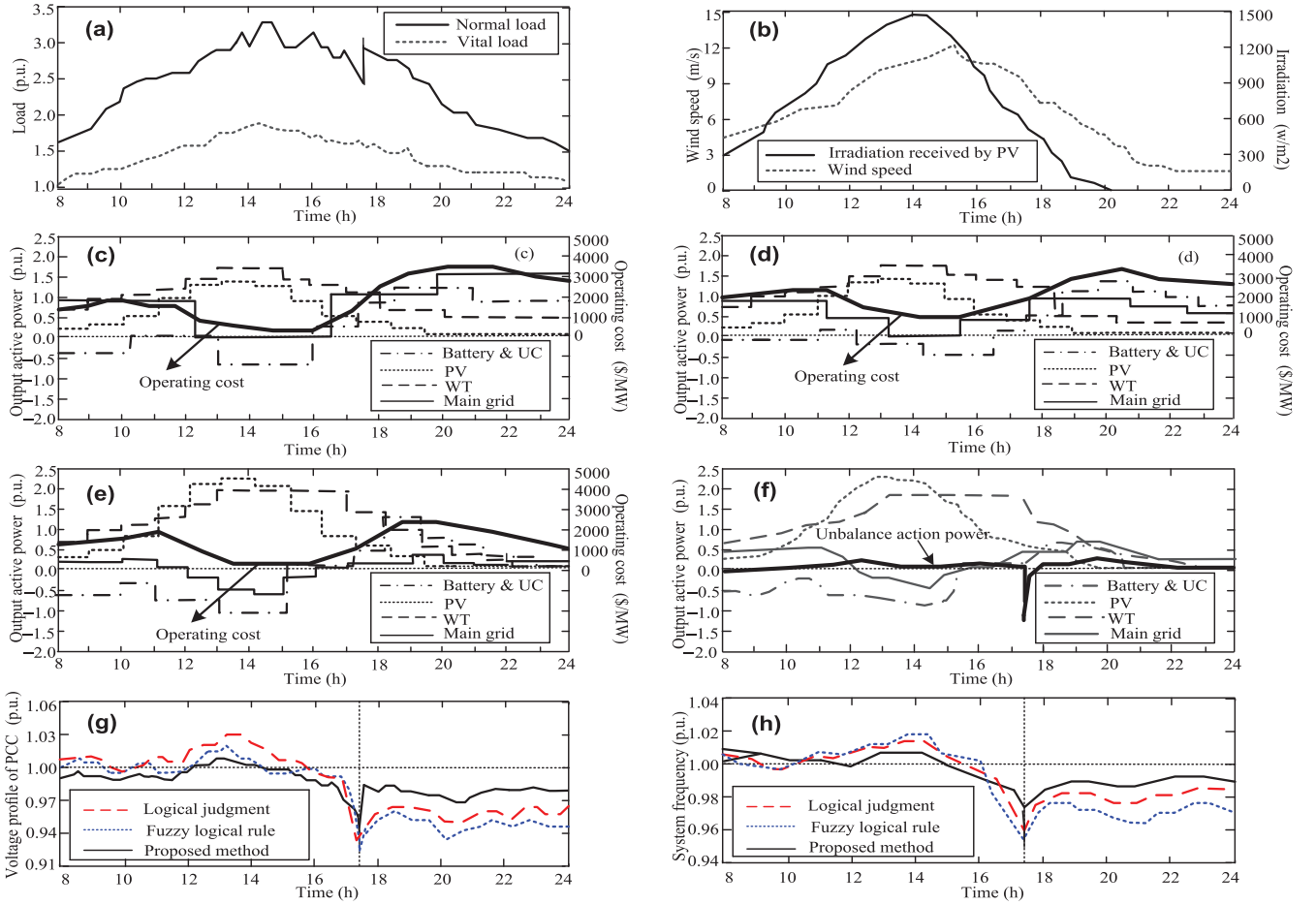

Fig. 5. Control performance of the HEGS. (a) Curves of loads. (b) Wind speed and sun irradiance. (c) Power dispatch and operating cost under the logical judgment-based scheme. (d) Power dispatch and operating cost under the fuzzy-logical rule-based scheme. (e) Power dispatch and operating cost under the proposed scheme. (f) Real power outputs and unbalance real power under the proposed scheme. (g) Voltage performance. (h) Frequency performance.

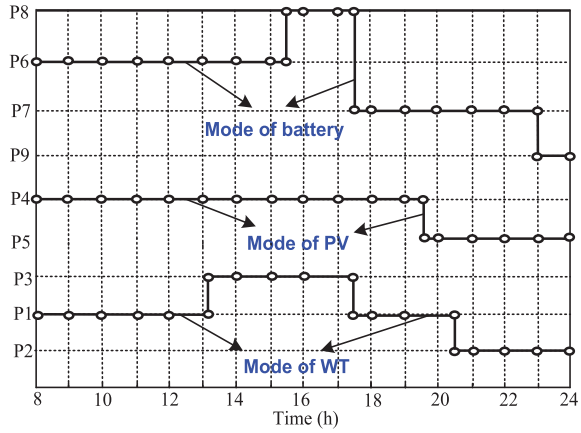

Fig. 6. Operation modes of three distributed generation units.

PCC voltage. Nevertheless, the PCC voltage can be regulated quickly within the range of 0.97 to 1.01 p.u., and the system frequency also can be maintained within the range of 0.99 to 1.01 p.u. Fig. 6 further shows the operation modes of all DERs when using the proposed control schemes.

It is worthwhile to mention that at 17:30 P.M., when the load disturbance occurs, the operation mode of the battery unit is switched by the coordinated switching control according to the coordinated logical relationship. The switching control is trigged by the PCC voltage assessment. In this manner, the PCC voltage can return quickly to the normal range. In another time slot, the mode is switched by the internal switching control, based on the constraint conditions of each unit.

The above simulation results imply that by means of the proposed schemes, two renewable energy units provide energy supply as much as possible so as to minimize operating cost of the system. In addition, they also indicate that the proposed switching control can ensure energy supply with higher reliability in response to the operation condition changes.

VII. Conclusion

This paper has developed a hierarchical management and control scheme based on MAS, allowing HEGS to provide a reliable, stable, and cost-effective power supply. In this work, the middle-level CCA is extended by using MAS, and the event-triggered hybrid switching controllers are designed by means of the DHPN model. This allows the operation mode of all DERs to be switched in a coordinated way when the operation condition changes. The simulation results indicate the HEGS has an increase in performance.

Compared with previous research results, the proposed scheme can switch the operation mode more intelligently and flexibly in the event of operational changes. Even though the model still relies on older communication systems, the dependency has been reduced due to the use of MAS. This approach of developing an EMS based on MAS allows the solution of constraints at the local level thereby reducing the computational and communication requirements. In brief, the MAS-based hierarchical energy management strategies is a suitable way to make complex HEGS smarter, where each energy resource and load are controlled by an intelligent autonomous agent, the middle-level agent executes coordinated switching control, and the upper-level agent implements the energy optimization management by using a common communications interface. It provides a feasible solution which combines artificial intelligence with mathematical tools to decide hybrid control actions. The MAS-based hierarchical energy management strategies can be easily applied to manage and control other kind of power systems such as smart grid and energy internet by extending the agents function and creating additional agent units.

REFERENCES

[1] J. Lagorse, D. Paire, and A. Miraoui, "Sizing optimization of a stand-alone street lighting system powered by a hybrid system using fell cell, PV and battery," *Renewable Energy*, vol. 34, no. 1, pp. 683–691, 2009.

[2] N. Hatziargyriou, H. Asano, R. Iravani, and C. Marnay, "Microgrids," *IEEE Power Energy Mag.*, vol. 5, no. 4, pp. 78–94, Jul./Aug. 2007.

[3] T. F. El-Shatter, M. N. Eskander, and M. T. El-Hagry, "Energy flow and management of a hybrid wind/PV/fuel cell generation system," *Energy Convers. Manage.*, vol. 47, no. 9–10, pp. 1264–1280, 2006.

[4] A. Hajizadehd and M. A. Golkar, "Intelligent power management strategies of hybrid distributed generation system," *Int. J. Elect. Power Energy Syst.*, vol. 29, no. 10, pp. 783–795, 2007.

[5] K.-S. Jeong, W.-Y. Lee, and C. S. Kim, "Energy management strategies of a fuel cell/battery hybrid system using fuzzy logics," *J. Power Sources*, vol. 145, no. 2, pp. 319–326, 2005.

[6] Z. H. Jiang, L. J. Gao, and R. A. Dougal, "Flexible multiobjective control of power converter in active hybrid fuel cell/battery power sources," *IEEE Trans. Power Electron.*, vol. 20, no. 1, pp. 245–254, Jan. 2005.

[7] Z. H. Jiang, L. J. Gao, and R. A. Dougal, "Adaptive control strategy for active power sharing in hybrid fuel cell/battery power sources," *IEEE Trans. Energy Convers.*, vol. 22, no. 2, pp. 507–515, Jun. 2007.

[8] D. B. Nelson, M. N. Nehrir, and C. Wang, "Unit sizing and cost analysis of stand-alone hybrid wind/PV/ fuel cell power generation system," *Renewable Energy*, vol. 31, no. 10, pp. 1641–1656, 2006.

[9] S. Ashok, "Optimised model for community-based hybrid energy system," *Renewable Energy*, vol. 32, no. 7, pp. 1155–1164, 2007.

[10] L. J. Gao, Z. H. Jiang, and R. A. Dougal, "An actively controlled fuel cell/battery hybrid to meet pulsed power demands," *J. Power Sources*, vol. 130, no. 1–3, pp. 202–207, 2004.

[11] C. X. Dou and B. Liu, "Hierarchical hybrid control for improving comprehensive performance in smart power system," *Int. J. Elect. Power Energy Syst.*, vol. 43, no. 1, pp. 595–606, 2012.

[12] S. Y. Jia and C. Jiang, "Design and implementation of MAS in renewable energy power generation system," in *Proc. 3rd Conf. Human Syst. Interact.*, Rzeszow, Poland, Jul. 2010, pp. 85–88.

[13] J. Zeng, J. F. Liu, J. Wu, and H. W. Ngan, "A multi-agent solution to energy management in hybrid renewable energy generation system," *Renewable Energy*, vol. 36, no. 5, pp. 1352–1362, 2011.

[14] J. Lagorse, M. G. Simoes, and A. Miraoui, "A multiagent fuzzy-logic-based energy management of hybrid systems," *IEEE Trans. Ind. Appl.*, vol. 45, no. 6, pp. 2123–2129, Nov./Dec. 2009.

[15] J. Lagorse, D. Paire, and A. Miraoui, "A multi-agent system for energy management of distributed power sources," *Renewable Energy*, vol. 35, no. 1, pp. 174–182, 2010.

[16] D. Wu, J. M. Guerrero, J. C. Vasquez, T. Dragicevic, and F. Tang, "Coordinated power control strategy based on primary-frequency- signaling for islanded microgrids," in *Proc. Energy Convers. Congr. Expo.*, Denver, CO, USA, Sep. 2013, pp. 1033–1038.

[17] Y. Wang and H. J. Mao, "Improved particle swarm optimization and its application in solving logistics deliver region partition model," in *Proc. Comput. Appl. Syst. Model.*, Taiyuan, China, Oct. 2010, pp. 481–486.

[18] S. Sotiriadis, N. Bessis, Y. Huang, P. Kuonnen, and N. Antonopoulos, "A JADE middleware for grid inter-cooperated infrastructures," in *Proc. IEEE Workshops Int. Conf. Adv. Inf. Netw. Appl.*, Singapore, Mar. 2011, pp. 135–140.

[19] V. K. Paruchuri, A. Davari, and A. Feliachi, "Hybrid modeling of power system using hybrid Petri net," in *Proc. 37th Southeastern Symp. Syst. Theory*, Mar. 2005, pp. 221–224.

[20] N. Lu, J. H. Chow, and A. A. Desrochers, "A multi-layer Petri net model for deregulated electric power systems," in *Proc. Amer. Control Conf.*, May 2002, pp. 513–518.

[21] J. Sun, S. Y. Qin, and Y. H. Song, "Fault diagnosis of electric power systems based on fuzzy Petri nets," *IEEE Trans. Power Syst.*, vol. 19, no. 4, pp. 2053–2059, Nov. 2004.

[22] J. M. Guerrero, M. Chandorkar, T. Lee, and P. C. Loh, "Advanced control architectures for intelligent microgrids—Part I: Decentralized and hierarchical control," *IEEE Trans. Ind. Electron.*, vol. 60, no. 4, pp. 1254–1262, Apr. 2013.

[23] J. M. Guerrero, P. C. Loh, T. Lee, and M. Chandorkar, "Advanced control architectures for intelligent microgrids—Part II: Power quality, energy storage, and AC/DC Microgrids," *IEEE Trans. Ind. Electron.*, vol. 60, no. 4, pp. 1263–1270, Apr. 2013.

[24] C. X. Dou and B. Liu, "Transient control for microgrid with multiple distributed generations based on hybrid system theory," *Int. J. Elect. Power Energy Syst.*, vol. 42, no. 1, pp. 408–417, 2012.

[25] C. X. Dou, B. Liu, and D. J. Hill, "Hybrid control for high-penetration distribution grid based on operational mode conversion," *IET Gener., Transmiss. Distrib.*, vol. 7, no. 7, pp. 700–708, 2013.

Junzhi Yu (SM'14) received the B.E. degree in safety engineering and the M.E. degree in precision instruments and mechanology from the North China Institute of Technology (currently North University of China), Taiyuan, China, in 1998 and 2001, respectively, and the Ph.D. degree in control theory and control engineering from the Institute of Automation, Chinese Academy of Sciences (IACAS), Beijing, China, in 2003.

He is currently a Professor with the State Key Laboratory of Management and Control for Complex Systems, IACAS. His research interests include biomimetic robots, intelligent control, and intelligent mechatonic systems.

Dr. Yu serves as an Associate Editor for the IEEE TRANSACTIONS ON ROBOTICS and the *Journal of Mechanical Science and Technology*, and as a Technical Editor for the IEEE/ASME TRANSACTIONS ON MECHATRONICS.

Chunxia Dou received the B.S. and M.S. degrees in automation from the Northeast Heavy Machinery Institute, Qiqihaer, China, in 1989 and 1994, respectively, and the Ph.D. degree in instrument science and engineering from Yanshan University, Qinhuangdao, China, in 2005.

In 2010, she joined the Department of Engineering, Peking University, Beijing, China, where she was a Postdoctoral Fellow for two years. Since 2005, she has been a Professor with the Institute of Electrical Engineering, Yanshan University, Qinhuangdao, China. Her research interests include multi-agent-based control, event-triggered hybrid control, distributed coordinated control, and multimode switching control, and their applications in power systems, microgrids, and smart grids.

Xinbin Li received the M.Sc. degree in control theory and control engineering from Yanshan University, Qinhuangdao, China, in 1999, and the Ph.D. degree in general and fundamental mechanics from Peking University, Beijing, China, in 2004.

Currently, he is a Professor with the Institute of Electrical Engineering, Yanshan University. His research interests include nonlinear systems and networked control systems.